A Fiber-Optic Accelerometer Based on Extrinsic Fabry-Perot Interference for Low Frequency Micro-Vibration Measurement

Peng Zhang, Shuang Wang, Junfeng Jiang, Zhiyuan Li, Haokun Yang, and Tiegen Liu

***Abstract*—A fiber-optic accelerometer based on extrinsic Fabry-Perot interferometer (EFPI) is reported. The sensor adopts flywheel diaphragm structure as a sensitive element, where the mass block is bonded in the center, while the beam of the flywheel acts as a spring. The sensitive element forms single degree of freedom spring-mass-damper system. The parameters of the accelerometer are designed based on finite element simulation (FEM), and the transfer function of the sensor is established by numerical simulation. The experiments indicate that the sensor has a wide detection frequency band with the detectable ability for micro-vibration low as 0.01 Hz, and the sensitivity is 7.02 rad/g @20 Hz, and reach an average sensitivity of 6.39 rad/g in 5–20 Hz. The research shows that the accelerometer has a good development prospect in the field of low frequency micro-vibration detection.**

***Index Terms*—Fiber optics systems, sensors.**

II. Introduction

In THE field of micro-vibration detection such as earthquake warning, the commonly used geophone is a type of low frequency accelerometer with wide frequency bands. It can detect seismic waves from a long distance, and of practical significance for source location and magnitude determination cooperated with the speedometer. At present, the commercial types of seismometers mainly include moving electrodynamic type, piezoelectric type and eddy-current type [1]–[6]. The seismic detection system formed by these devices has some problems, such as power supply demand, easy to be interfered with electromagnetic, which restrict the development of seismic early warning technology to a certain extent. In addition, in the fields of spacecraft [7], [8], perimeter security [9], [10] and vehicle condition monitoring [11], the measurement of micro-vibration acceleration has always been the focus of researchers.

Manuscript received 7 May 2022; revised 12 June 2022; accepted 13 June 2022. Date of publication 16 June 2022; date of current version 4 July 2022. This work was supported by the National Natural Science Foundation of China under Grants 62075160, 61735011, and U2006216. *(Corresponding authors: Shuang Wang; Junfeng Jiang.)*

The authors are with the School of Precision Instrument and Opto-electronics Engineering, Tianjin University, Tianjin 300072, China, also with the Key Laboratory of Opto-electronics Information Technology, Tianjin University, Tianjin 300072, China, and also with the Ministry of Education and Tianjin Fiber-Optic Sensing Engineering Center, Institute of Fiber-Optic Sensing of Tianjin University, Tianjin 300072, China (e-mail: zp90731@tju.edu.cn; shuangwang@tju.edu.cn; jiangjfjxu@tju.edu.cn; zhiyuanli@tju.edu.cn; yanghaokun@tju.edu.cn; tgliu@tju.edu.cn).

Digital Object Identifier 10.1109/JPHOT.2022.3183438

The use of accelerometers based on mechatronic structures remains commoner in the industry. Nevertheless, the research on fiber-optic accelerometers has been ongoing.

Fiber-optic accelerometer is suitable for geophysical research in complex environment because of its advantages of anti-electromagnetic interference, high sensitivity, strong environmental tolerance and mature multiplexing technology. The research on fiber-optic accelerometer started earlier in the industry. In the 1980s, Glen A. Rines *et al.* [12] proposed a fiber-optic accelerometer based on cantilever beam structure. Since then, A. S. Gerges *et al.* [13], [14] have reported several fiber-optic accelerometers based on Fabry-Perot (F-P) interference, and David A. Brown *et al.* [15] have also reported a type of push-pull fiber-optic accelerometer based on Michelson interferometer. The above reports suggest that fiber-optic accelerometer has a good development prospect. In recent years, with the development of grating etching, femtosecond laser processing, micro-electro-mechanical system and other technologies, a variety of fiber accelerometers with high precision and multi-parameter measurement function have been reported. For instance, W. Zhang *et al.* [16] reported a kind of sensor which realized double parameter measurement of acceleration and magnetic intensity based on F-P interference and a kind of fiber Bragg grating based accelerometer. Q. Yu *et al.* [17] reported F-P accelerometer based on fast white light interference. The accelerometer based on F-P interference can detect vibration signals as low as 10 Hz, while J. Chen *et al.* [18], [19] also conduct in-depth research on the accelerometers based on Michelson interferometer. Based on such structure, the measurable lower limit frequency of the accelerometer can reach 0.005 Hz, while the optical path of the system is relatively complex and need high implementation cost. With regard to micro-vibration detection, for example, seismic wave monitoring, the frequency range of accelerometers needs to be lower as 0.01 Hz, so as to be able to monitor some long-period vibration signals. Therefore, the way to achieve low frequency detection needs to become the focus of research for accelerometers in the field of fiber-optic sensing.

A fiber-optic acceleration sensor based on EFPI is proposed. We introduce the basic principle, design the specific parameters and establish the transfer function model of the sensor by using FEM and numerical simulation. The micro-vibration acceleration measurement and sensitivity calibration experiment were carried out on the vibration platform.

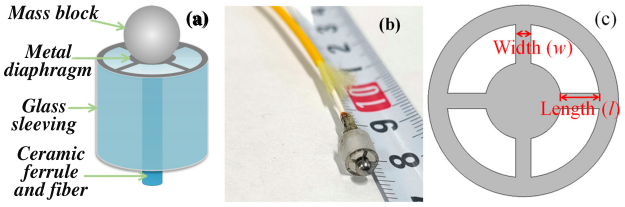

Fig. 1. (a) Structure of the sensor, (b) Image of the sensor (c) Structure of the flywheel diaphragm.

II. Design, Simulation and Fabrication

A kind of accelerometer suitable for low frequency micro-vibration acceleration measurement based on EFPI is demonstrated. The structure of the sensor is shown in Fig. 1(a). We utilize the metal diaphragm with the mass block as the sensitive element. The metal diaphragm is flywheel type, and its structure is shown in Fig. 1(c). A small steel ball is attached to the outside of the central diaphragm as the mass block, and its weight is much greater than the metal diaphragm. The central diaphragm is connected by four beams to the outer ring, which stick the diaphragm on the glass sleeving. The ceramic ferrule of the fiber is also fixed in the glass sleeving, thus formed a F-P cavity, and the reflective surfaces of which are the inner side of center diaphragm and the fiber end face respectively.

For the structure of sensitive element, it can be equivalent to the single degree of freedom spring-mass-damper system. Mass block m is connected to a spring with elastic coefficient k and a damper with damping coefficient c. Given the motion of the measured object be $Y(t) = Y_0 \sin\omega t$, when the system is in stable state, the differential equation of system motion is [18], [20], [21],

$$m\ddot{x}(t) + c\dot{x}(t) + kx(t) = m\ddot{Y}(t) \tag{1}$$

And for the sake of presentation, (1) is written in terms of (2),

$$\ddot{x}(t) + 2\xi\omega_0\dot{x}(t) + \omega_0^2 x(t) = Y_0\omega_0^2 \sin\omega t \tag{2}$$

where $\xi = c/2\sqrt{mk}$,$\omega_0 = \sqrt{k/m}$. ξ is damping ratio and ω_0 is resonant angular frequency of the system.

It is pointed out in [18] that in the case of low frequency measurement, i.e., when $\omega << \omega_0$, the special solution z of (2) can be simplified as,

$$z \approx \frac{1}{\omega_0^2}\omega^2 Y_0 \sin\omega t \tag{3}$$

This shows that at low frequency band, the output of the system is proportional to the acceleration of the applied vibration.

As for the transfer function, generally, the transfer function $H(s)$ is given by,

$$H(s) = \frac{\omega_0^2}{s^2 + 2\xi\omega_0 s + \omega_0^2} \tag{4}$$

where $\xi = c/2\sqrt{mk}$, $\omega_0 = \sqrt{k/m}$, $s = \mathrm{j}\omega$. ξ is damping ratio and ω_0 is resonant angular frequency of the system. According to [18], [20], [21], when ω_0 is much less than ω, the amplitude-frequency characteristic, the value of $|H(\mathrm{j}\omega)|$ is close to 1, that is, when the resonant angular frequency of the vibration sensor ω_0 is much greater than the vibration frequency ω to be measured, the acceleration sensitivity is approximately a constant.

In the system, the performance of the transfer function in the passband can be adjusted by modifying parameters including c, m, and k. Parameter c is the damping coefficient which is an important value for calculating ξ. It has been reported in [18] that geophones generally work under the condition of underdamping. In this study, we set the value of ξ as 0.1. From another point of view, the damping coefficient c does not affect the resonant angular frequency, thus the adjustment of the resonant frequency should be focused on m and k. The mass block m is the mass of the steel ball attached to the flywheel diaphragm. k is the elastic coefficient of the flywheel diaphragm beam. The value of k should be $k = nEwh^3l^{-3}$ [22]–[24], where n is the number of the flywheel beams of diaphragm, E is the Young's modulus of the diaphragm material, w, l and h are the width, length and thickness of the flywheel beam respectively.

According to the analysis above, decreasing the elastic coefficient k or increasing the mass block m can make the resonant frequency close to the low frequency band. If the mass is too large, the static deformation of the diaphragm will be large. Meanwhile, the thickness and bearing capacity of the diaphragm should be taken into account. It must be emphasized that reducing the intrinsic frequency does not mean that the lower the intrinsic frequency of the sensor is better. According to the above analysis, the intrinsic frequency should be at least five times greater than the frequency we are interested in. In this case, the accelerometer works in theory. Refer to the expression $k = nEwh^3l^{-3}$ for k, the effective way to reduce k by order of magnitude is to increase the length of the beam l, reduce the width of beam w.

In order to analyze the influence of different diaphragm structures on the intrinsic frequencies, the intrinsic frequencies under different diaphragm structure parameters are analyzed by COMSOL simulation software. The conditions that set for the four-beam diaphragm simulation are $m = 0.11$ g, $h = 0.01$ mm, l = [1.0, 1.5] (unit: mm), w = [0.2, 0.9](unit: mm). Fig. 2 shows the simulation results of the intrinsic frequency of the diaphragm. It should be noted that h also has an impact on the local vibration frequency of the structure, but from an order of magnitude, "h^3" has a greater impact. Therefore, we carried out the FEM simulation on the premise of preliminarily determining the most suitable thickness h of the diaphragm.

Considering the need of low frequency measurement, FEM simulation of resonant frequency of metal diaphragm is carried out. Too high resonant frequency will make the sensor very insensitive to the corresponding low frequency signal in direct test, while, too low intrinsic frequency will make the accelerometer theoretically untenable, so it is necessary to adjust the structural parameters of the diaphragm to find the most suitable resonant frequency. When the structural parameters are [$h = 0.01$ mm, $w = 0.5$ mm, $l = 1$ mm], the first-order natural frequency of the four-beam sensitive diaphragm is 109.92 Hz. Under such conditions, the sensor can better meet the requirements of normal operation.

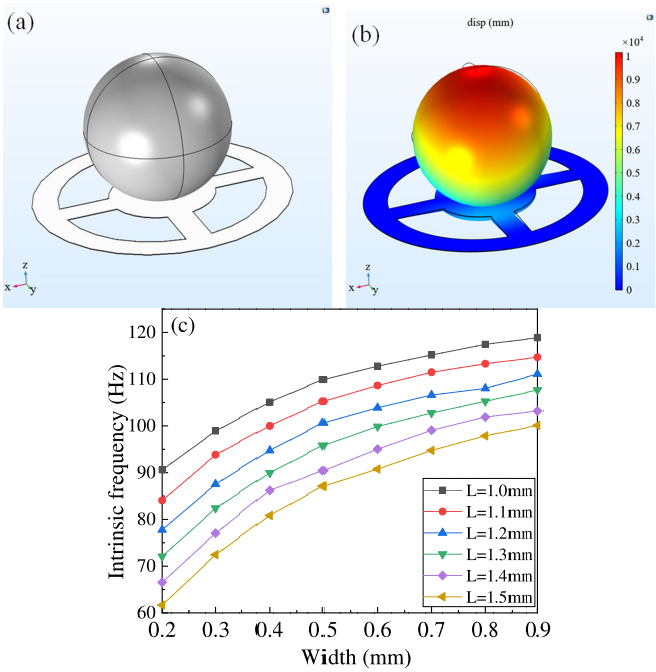

Fig. 2. (a) Geometric model of the sensor (b) FEM intrinsic frequency simulation (c) Intrinsic frequency simulation under different length L and width w.

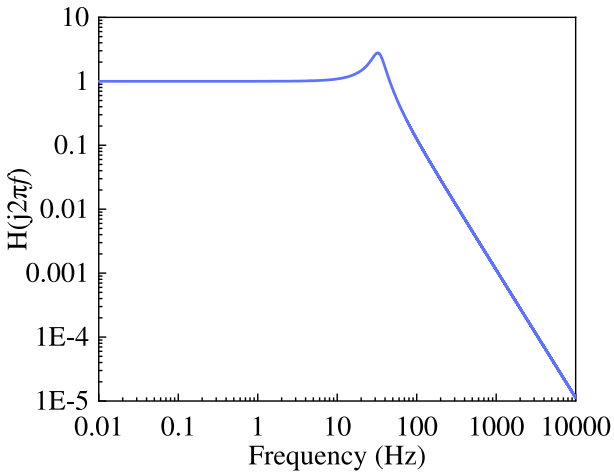

Fig. 3. Numerical simulation of amplitude-frequency characteristics.

Based on the above conditions, the amplitude-frequency characteristics $|H(\mathrm{j}2\pi f)|$ of the sensor transfer function were analyzed and illustrate in Fig. 3, and the working frequency was set at 10^{-2}–10^{4} Hz. Meanwhile, the intrinsic frequency of the system is 115.47 Hz through numerical calculation, which is close to the results of FEM simulation. Based on previous research on effective working frequency bands, the working frequency of the acceleration sensor can theoretically be 20 Hz and below.

III. Experimental Results and Discussion

The interference spectrum of the F-P cavity of the sensor was tested when utilizing SLD source with Gaussian spectrum, as shown in Fig. 4, and the initial cavity length of the cavity is 64.5 um according to double-peak phase demodulation [25].

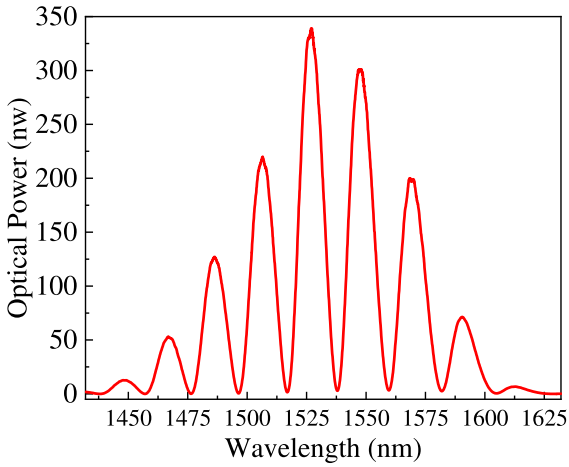

Fig. 4. Interference spectrum of F-P accelerometer sensor.

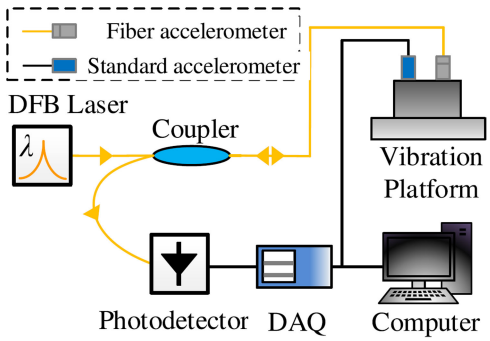

Fig. 5. Experimental setup for low frequency micro-vibration based on intensity demodulation.

The intensity demodulation system was used for experimental study of acceleration measurement. The intensity of reflected signal of F-P interference, which is approximately two-beam interference, is given by,

$$I = 2RI_0\left[1-\cos\left(\frac{4\pi L}{\lambda}\right)\right] \tag{5}$$

where I is the intensity of the signal reflected by the sensor, I_0 is the intensity of the incident light, R is the reflectivity of interfaces, L is the length of the F-P cavity, and λ is the central wavelength of the DFB laser. When using intensity demodulation, we expect the sensor to work within the $\pi/4$ linear range centered on the maximum point of derivative of sinusoidal interference curve [26]. The expected cavity length of the sensor is analyzed according to (5), and the cavity length L should meet the following condition,

$$L = \frac{\lambda}{4}\left(k+\frac{1}{2}\right),\ k = 0, 1, 2 \tag{6}$$

The initial cavity length of the sensor is close to $L = 64.51\ \mu$m when $k = 167$, which indicates that the sensor can be demodulated normally by the intensity demodulation method.

The experimental setup is shown in Fig. 5. The system includes a distributed feedback (DFB) laser source, a 1 × 2 coupler, vibration platform (Beijing Yiyang Co., Ltd, YE5), fiber-optic EFPI accelerometer and standard accelerometer (Shanghai Yakoon Co., Ltd., YD10), InGaAs amplified photodetector (Thorlabs Inc., PDA10CS-EC) and data acquisition (DAQ) card (National Instruments Corp., USB6002). The fiber-optic accelerometer and the standard accelerometer are fixed on the vibration platform. The narrow-bandwidth pulse center wavelength generated by DFB laser is 1550.12 nm. The pulse enters the fiber-optic accelerometer through the 3 dB coupler and interferes in the F-P cavity formed by the end face of the fiber-optic and the inner surface of the diaphragm. Then the interference light is transmitted to the photoelectric detector for photoelectric conversion, which is convenient for data storage and demodulation.

According to the actual measurement requirements, we hope that the accelerometer has detection ability at the low frequency band. The vibration period is set to 100 s, 50 s, 20 s, 10 s, 5 s, 2 s respectively, and the cosine excitation voltage of the vibration platform is set at 200 mV. It should be noted that the standard accelerometer used in the experiment cannot measure the vibration acceleration signal lower than 0.5 Hz, so we describe the driving voltage applied to the vibration platform and its period instead. Based on this, the low frequency micro-vibration acceleration experiment is carried out and the phase demodulation results are shown in Fig. 6(a), and the fast Fourier transform (FFT) of phase results are illustrated in Fig.6(b), which shows the frequency domain information. In Fig.6(a), the phase curve is somewhat unsmooth, which may be due to the nonlinear response of the sensor, the power frequency vibration of the vibration platform and the fluctuation of the demodulation system. In the reported literatures [16], [17], [27], the lowest frequency that can be measured by sensors based on fiber-optic EFPI is generally not less than 10 Hz. To some extent, the performance of fiber-optic accelerometer in low frequency band is a breakthrough in this area of research.

The sensitivity characteristics of accelerometer are analyzed, and the sensitivity of acceleration sensor is defined as the slope of linear regression line of acceleration phase. The frequency of the excitation voltage of the vibration platform was set at 10 Hz, and the peak-to-peak value of the cosine excitation voltage gradually increased at 20 mV intervals from 100 mV to 400 mV. Then the test results of standard accelerometer and phase demodulation data of fiber-optic EFPI accelerometer are analyzed, what we select is also the peak-to-peak values of the aforementioned two kinds of sensors. Under cosine voltage excitation of 10 Hz and 100–400 mV, corresponding scatter diagram of acceleration and radian is shown in Fig.7(a) as yellow dots. Similarly, the scatter diagram of acceleration and radian at 20 Hz is shown in Fig.7(b). The sensitivity of the sensor is analyzed by linear regression, and the linear regression line is shown as blue line in Fig. 7. The sensitivity values of the sensors are 5.92 rad/g @10 Hz and 7.02 rad/g @20 Hz respectively, and the goodness of fit was 0.9920 and 0.9986 correspondingly. Besides, the absolute errors between the acceleration value calculated from the linear fitting line and the acceleration measurement value are analyzed,

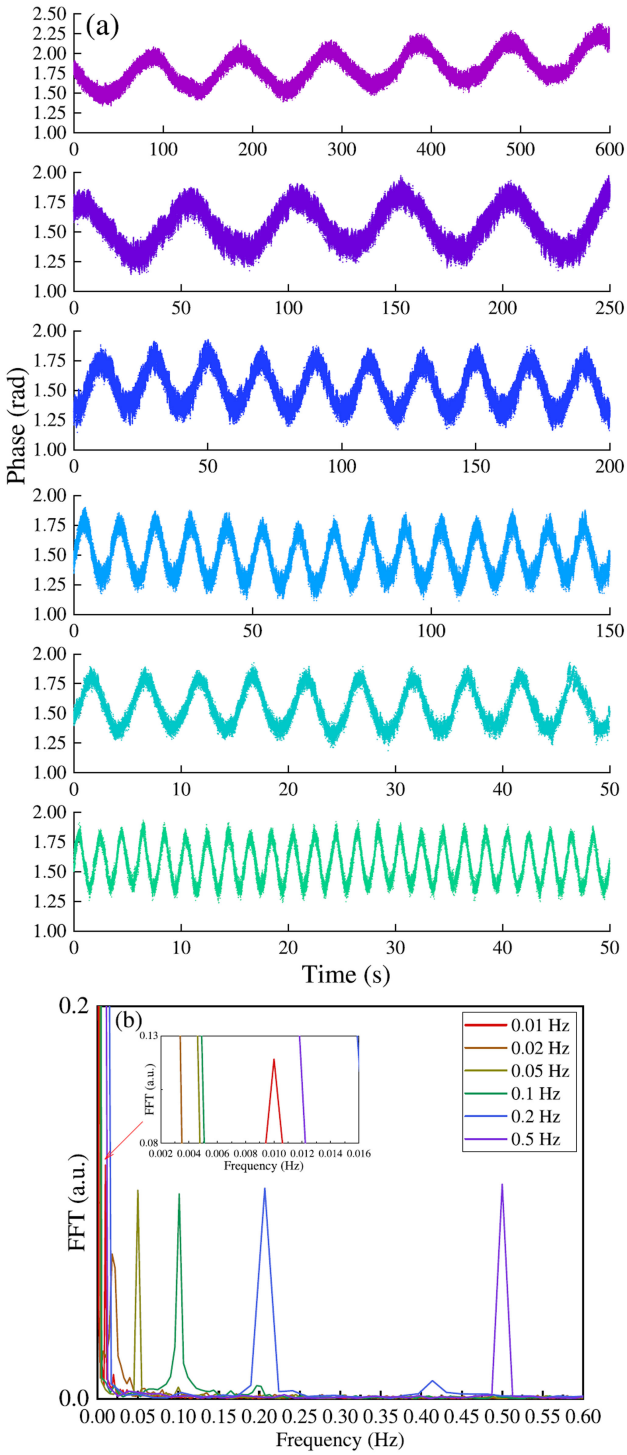

Fig. 6. (a) Phase demodulation curves of low frequency micro-vibration under input voltage excitation with frequency of 0.01, 0.02, 0.05, 0.1, 0.2, 0.5 Hz from top to bottom, (b) FFT of phase results with excited frequency of 0.01, 0.02, 0.05, 0.1, 0.2, 0.5 Hz.

and the corresponding illustration of the absolute error of each acceleration value are shown in the Fig. 7.

In the same way, the sensitivity values of sensor under micro-vibration excitation of other positive integer frequencies in the range of 5–20 Hz are analyzed, and the results are plotted in Fig. 8. The mean sensitivity in this frequency range was

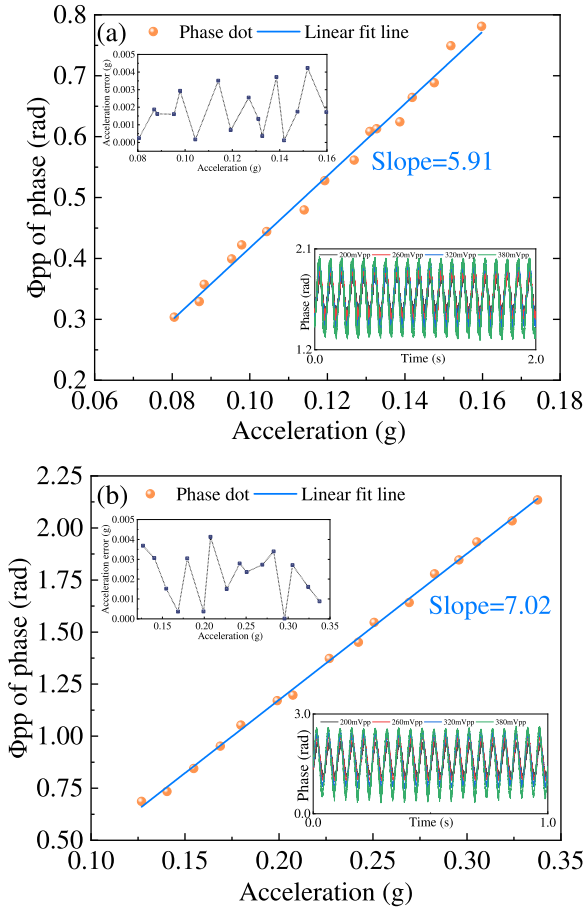

Fig. 7. Scatter plot of accelerometer measurement results and peak-to-peak (Φpp) phase demodulation results and linear fitting analysis of (a)10 Hz, (b) 20 Hz with acceleration error and demodulated phase results under excited voltage of 200, 260, 320 and 380 mVpp.

6.39 rad/g with the mean absolute deviation of 0.438 rad/g, and the sensitivity of the sensor fluctuate in the range of 5.77–7.26 rad/g @ 5–20 Hz. Similarly, an illustration of maximum absolute acceleration error in the range of 5–20 Hz is also shown in Fig. 8, and the maximum absolute acceleration error is the maximum values obtained from the error analysis of a single frequency such as 10, 20 Hz provided above. Although the sensitivity within this range is relatively close, the consistency still needs to be improved. Therefore, for the vibration of a specific frequency, the most appropriate way is to use the sensitivity corresponding to the frequency in Fig. 8 and its linear fitting line to calculate its acceleration value in order to accurately obtain the acceleration by the phase. As mentioned in II, the working frequency band of the sensor should be much lower than its resonant frequency in theory, and the frequency band is generally selected at 1/5 or below the resonant frequency. Therefore, we believe that the maximum working frequency of the fiber-optic EFPI acceleration sensor is more appropriate at 20 Hz. It has to be admitted that although the sensitivities of the sensor at different frequencies are close, there are still some errors, which may be caused by the nonlinear vibration of the fiber-optic sensor, the error of the standard sensor, the irregular vibration of the vibration platform itself and so on.

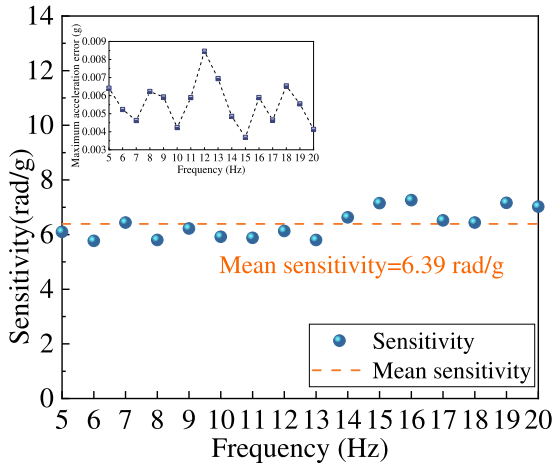

Fig. 8. Acceleration sensitivity and maximum error of 5–20 Hz micro-vibration.

Therefore, our future work will focus on the optimization of the physical parameters of the sensor and the optical demodulation system to improve the accuracy of sensitivity and better adapt to the practical application of low-frequency micro-vibration measurement.

IV. Conclusion

The fiber-optic EFPI accelerometer proposed in the paper is designed based on single degree of freedom spring-mass-damping system. The sensitive diaphragm of the sensor adopts fly-wheel structure and its structural parameters are designed around the intrinsic frequency of the sensitive diaphragm. Experiments show that the sensor has a good frequency response below 20 Hz, its acceleration sensitivity reaches 5.92 rad/g @ 10 Hz and 7.02 rad/g @ 20 Hz respectively, and reach an average sensitivity of 6.39 rad/g in 5–20 Hz. It can detect acceleration signals as low as 0.01 Hz. Our sensor greatly expands the detection range of fiber-optic EFPI accelerometer. The sensor has a good application prospect in seismic monitoring, mineral exploration and other occasions requiring low frequency micro-vibration acceleration measurement.

References

[1] Y. S. Lu, H. W. Wang, and S. H. Liu, "An integrated accelerometer for dynamic motion systems," *Measurement*, vol. 125, pp. 471–475, 2018.
[2] Y. W. Hsu *et al.*, "A capacitive low-g three-axis accelerometer," in *Proc. 10th Int. Conf. Electron. Mater. Packag.*, 2008, pp. 325–328.
[3] Q. Zhang *et al.*, "Research on the monolithic micromachined accelerometer array sensor in the field of nuclear power generation," *Sensor Lett.*, vol. 11, no. 11, pp. 2189–2191, 2013.
[4] L. Song, H. Huang, and W. Wang, "Principle of electrodynamic active servo feedback accelerometer with single coil," *World Earthq. Eng.*, vol. 26, no. 3, pp. 188–190, 2010.
[5] J. H. Kim, Y. G. Lee, and C. G. Kim, "An experimental study on a new air-eddy current damper for application in low-frequency accelerometers," *J. Mech. Sci. Technol.*, vol. 29, no. 9, pp. 3617–3625, 2015.
[6] G. Zhao, C. Liu, and H. Jiang, "Principle and use of kind of angle-displacement eddy-current transducer," *Instrum. Technique Sensor*, vol. 7, no. 7, pp. 1–3, 2004.
[7] Z. Wang *et al.*, "Measurement of spacecraft micro-vibration based on quartz-flexibility-accelerometer," *Spacecraft Environ. Eng.*, vol. 33, no. 2, pp. 199–205, 2016.

[8] G. Ma *et al.*, "Calibration of the high accuracy acceleration sensor used in micro-vibration test," *Spacecraft Environ. Eng.*, vol. 35, no. 2, pp. 170–177, 2018.
[9] M. M. Khan and R. K. Sonkar, "Design and proposal of dual line-of-defense perimeter watchdog incorporating optimally designed FBG based accelerometers and strain sensors using single optical fiber," in *Proc. Int. Conf. Opt. Photon.*, 2015, vol. 9654, pp. 217–224.
[10] A. Davis and H. Chang, "Airport protection using wireless sensor networks," in *Proc. IEEE Int. Conf. Technol. Homeland Secur.*, 2012, pp. 36–42.
[11] Q. Wang *et al.*, "Research on application of micro-nano acceleration sensor in monitoring the vibration state of vehicles," *Int. Workshop Inf. Electron. Eng.*, vol. 29, pp. 1213–1317, 2012.
[12] G. A. Rines *et al.*, "Fiber-optic accelerometer with hydrophone applications," *Appl. Opt.*, vol. 20, no. 19, pp. 3453–3459, 1981.
[13] S. Gerges *et al.*, "A hemispherical air cavity fibre Fabry-Perot sensor," *Opt. Commun.*, vol. 68, no. 3, pp. 157–160, 1988.
[14] S. Gerges *et al.*, "High-sensitivity fiber-optic accelerometer," *Opt. Lett.*, vol. 14, no. 4, pp. 251–253, 1989.
[15] D. A. Brown and S. L. Garrett, "Interferometric fiber optic accelerometer," in *Proc. Int. Soc. for Opt. Eng.*, 1991, vol. 1367, pp. 282–288.
[16] Z. Wang *et al.*, "A fiber optic accelerometer-magnetometer," *J. Lightw. Technol.*, vol. 35, no. 9, pp. 1732–1737, May 2017.
[17] Z. Zhao *et al.*, "A fiber-optic Fabry-Perot accelerometer based on high-speed white light interferometry demodulation," *J. Lightw. Technol.*, vol. 36, no. 9, pp. 1562–1567, 2018.
[18] J. Chen *et al.*, "Ultra-low frequency tri-component fiber optic interferometric accelerometer," *IEEE Sens. J.*, vol. 18, no. 20, pp. 8367–8374, Oct. 2018.
[19] J. Chen *et al.*, "Method for determining the resonance frequency of a fiber optic interferometric accelerometer," *IEEE Trans. Instrum. Meas.*, vol. 67, no. 3, pp. 698–705, Mar. 2018.
[20] H. L. Wang *et al.*, "Fiber grating acceleration vibration sensor with double uniform strength cantilever beams," *J. Optoelectron. Laser*, vol. 24, no. 4, pp. 635–641, 2013.
[21] H. L. Wang *et al.*, "Characteristics of low-frequency vibration FBG sensor," *J. Optoelectron. Laser*, vol. 23, no. 6, pp. 1023–1030, 2012.
[22] X. G. Qi *et al.*, "Flywheel-like diaphragm-based fiber-optic Fabry–Perot frequency tailored acoustic sensor," *J. Phys. D: Appl. Phys.*, vol. 53, no. 41, 2020, Art. no. 415102.
[23] S. Saxena, R. Sharma, and B. D. Pant, "Dynamic characterization of fabricated guided two beam and four beam cantilever type MEMS based piezoelectric energy harvester having pyramidal shape seismic mass," *Microsystem Technol.*, vol. 23, no. 12, pp. 5947–5958, 2017.
[24] S. Saxena, R. Sharma, and B. D. Pant, "Design and development of guided four beam cantilever type MEMS based piezoelectric energy harvester," *Microsystem Technol.*, vol. 23, no. 6, pp. 1751–1759, 2017.
[25] M. S. Cheri *et al.*, "Fabrication, characterization, and simulation of a cantilever-based airflow sensor integrated with optical fiber," *Appl. Opt.*, vol. 52, no. 14, pp. 3420–3427, 2013.
[26] P. Zhang *et al.*, "Mechanical filter-based differential pressure fiber-optic Fabry-Perot infrasound sensor," *IEEE Photon. J.*, vol. 13, no. 3, Jun. 2021, Art. no. 6800110.
[27] S. Li *et al.*, "Low-cost fiber optic extrinsic Fabry-Perot interferometer based on a polyethylene diaphragm for vibration detection," *Opt. Commun.*, vol. 457, 2020, Art. no. 124332.